Journal of Nuclear Materials 399 (2010) 13–25

Contents lists available at ScienceDirect

Journal of Nuclear Materials

journal homepage: www.elsevier.com/locate/jnucmat

Raman and X-ray absorption spectroscopic studies of hydrothermally altered alkali-borosilicate nuclear waste glass

David A. McKeown *, Andrew C. Buechele, Carol Viragh, Ian L. Pegg

Vitreous State Laboratory, The Catholic University of America, 620 Michigan Ave., N.E., Washington, DC 20064, United States

ARTICLE INFO

Article history:
Received 8 May 2009
Accepted 9 December 2009

ABSTRACT

Raman spectroscopy and X-ray absorption spectroscopy (XAS) are used to characterize structural changes that took place in hydrothermally altered (Na,K)-alumina-borosilicate glasses with different Na/K ratios, formulated as part of a durability study to investigate the behavior of glasses for nuclear waste storage. The hydrothermal experiments, or vapor hydration tests (VHT), were performed on each glass for 3 and 20 days at 200 °C to accelerate and approximate long-term alteration processes that may occur in a nuclear waste repository. Results found for both glasses and their VHT altered counterparts show little, if any, structural influence from the different starting Na/K ratios. X-ray diffraction, differential scanning calorimetry, scanning electron microscopy, and Raman spectroscopy indicate that the altered samples are mostly amorphous with small amounts of analcime-like and leucite-like crystals within 200 μm of the sample surface and contain up to 9.7 wt.% water or OH. The Raman data are nearly identical for the amorphous portions of all altered VHT samples investigated, and indicate that two glass structural changes took place during alteration: one, partial depolymerization of the alumina-borosilicate network, and two, introduction of water or OH. Al and Si XAS data indicate tetrahedral AlO_4 and SiO_4 environments in the original glasses as well as in the altered samples. Small energy shifts of the Si K-edge also show that the altered VHT samples have less polymerized networks than the original glass. Na XAS data indicate expanded Na environments in the VHT samples with longer Na–O distances and more nearest-neighbor oxygen atoms, compared with the original glasses, which may be due to hydrous species introduced into the expanding Na-sites.

1. Introduction

1.1. Glass characteristics and corrosion experiments

The two glasses investigated are part of a matrix of 12 simplified alkali-alumina-borosilicate glass compositions based on actual waste glass compositions developed to vitrify high-sodium, low-activity nuclear waste (LAW) at the Hanford site [1]. The simplified matrix was designed to study variations in vapor hydration test (VHT (ASTM C1663)) durability [2,3] produced by alkali substitution (K for Na in two steps), and by successive additions of Fe, Mg, and Ca. The two glasses studied here, Lo1A and Lo2A [1], were at the high-Na extreme of the test matrix, and have the same composition except that in Lo2A glass, the K_2O concentration is increased at the expense of Na_2O (Table 1). Data provided by testing such simplified glasses are useful as indicators of how similar variations in more complex actual waste-glass formulations will affect their VHT durability.

The VHT is one of the product quality requirements for vitrified LAW from the Hanford site and is employed in assessing the durability of waste-glasses under aqueous attack during long-term storage [2]. The VHT used here [3], is a highly accelerated test, because test conditions are far more severe (slightly oversaturated water vapor at 200 °C) than are likely to be experienced by a waste-glass during actual storage. Nuclear waste-glasses will need to be stored for thousands of years, or orders of magnitude greater than practical test durations. Short tests at projected actual or probable humidity and temperature during storage provide an extremely limited basis from which to estimate long-term durability. Accelerated tests are used to enhance the rates of the reactions, which take place and corrode the glass as a result of its contact with water. The results of accelerated tests provide data within practical time frames that can be used to enhance confidence in predicting long-term waste-glass durability.

In this study, each glass was exposed to a hydrous atmosphere at 200 °C for 3 and 20 days. The glasses investigated are of particular interest, because the 20-day VHT experiments altered each sample to the point where the original glass wafer softened, flowed from its wire support, and was found re-solidified at the bottom of the VHT vessel. This behavior is thought to be due to extensive up-

* Corresponding author. Tel.: +1 202 319 5226; fax: +1 202 319 4469.
E-mail address: davidm@vsl.cua.edu (D.A. McKeown).

0022-3115/$ - see front matter © 2009 Elsevier B.V. All rights reserved.
doi:10.1016/j.jnucmat.2009.12.007

Table 1
Major oxide compositions of representative areas within the original glasses and corresponding VHT altered samples from XRF and SEM–WDS analyses (wt.%), respectively. Crystalline phase compositions are from SEM–EDS (wt.%). One σ standard deviation listed in parentheses.

Sample	Na_2O	K_2O	Network formers	Al_2O_3/SiO_2	Total
Lo1A glass	20.81 (0.95)	0.51 (0.04)	Al_2O_3 6.02 (0.08) B_2O_3 9.02 (0.13) SiO_2 63.64 (0.79)	0.095	100.0
Lo1A C2D3 (altered glass)	16.90 (1.94)	0.63 (0.02)	Al_2O_3 5.98 (0.12) B_2O_3 11.05 (1.57) SiO_2 62.65 (0.99)	0.095	96.06
Lo1A C2D20 (altered glass)	15.93 (0.57)	0.79 (0.01)	Al_2O_3 6.09 (0.01) B_2O_3 10.59 (0.57) SiO_2 63.77 (0.02)	0.095	96.03
Lo2A glass	18.30 (1.04)	2.49 (0.12)	Al_2O 5.79 (0.32) B_2O_3 8.19 (0.37) SiO_2 65.23 (1.13)	0.089	100.0
Lo2A C2D3 (altered glass)	8.81 (1.36)	1.90 (0.14)	Al_2O_3 5.42 (0.08) B_2O_3 10.43 (1.59) SiO_2 64.40 (0.86)	0.084	90.96
Lo2A C2D20 (altered glass)	10.07 (0.78)	1.72 (0.07)	Al_2O_3 6.18 (0.11) B_2O_3 9.20 (0.42) SiO_2 64.93 (1.39)	0.095	92.09
Lo2A C2D20 analcime-like crystal (Fig. 2b point 1)	10.23 (0.18)	0.52 (0.05)	Al_2O_3 17.29 (0.21) SiO_2 71.96 (0.36)	0.240	100.0
Lo2A C2D20 leucite-like crystal (Fig. 2b point 2)	2.82 (0.11)	15.42 (0.12)	Al_2O_3 11.41 (0.17) SiO_2 70.31 (0.32)	0.162	99.96

take of water. Due to this amount of alteration, Raman and X-ray absorption spectroscopies are used to investigate how the glass structure changed as a result of exposure to the VHT conditions.

Earlier corrosion studies of silicate glasses and minerals in powder or bulk form [4–7] show that a variety of crystalline phases, such as analcime (nominally, $NaAlSi_2O_6{\cdot}H_2O$), merlinoite ($(K; Ca; Na; Ba)_7Si_{23}Al_9O_{64}{\cdot}23H_2O$), as well as other phyllosilicates and zeolites, can crystallize from an original glass during the alteration process. Using NMR techniques [6], Al coordination changes were also found by observing AlO_4 tetrahedra in the original crystal and glass powders, while significant populations of AlO_6 octahedra were found in the altered layers of the corresponding corroded samples. Compared with the original glass, increased silicate tetrahedral polymerization and silica enrichment in conjunction with Na and B depletion were observed in the altered outer surface layers of the glass samples [4,7].

1.2. Raman spectroscopy

For this study, Raman data were collected for two minerals, analcime and leucite ($KAlSi_2O_6$), since minor amounts of similar phases are found in the altered VHT samples as determined from X-ray diffraction (XRD) and scanning electron microscopy–energy dispersive spectroscopy (SEM–EDS) (Figs. 1, 2a and b, as well as Table 1, bottom two rows). The corresponding crystal structures have the same fully polymerized aluminosilicate tetrahedral framework of inter-connected four- and six-membered tetrahedral rings [8,9]. Differences are found in the alkali sites that are occupied by Na in analcime, and K in leucite. In analcime, H_2O molecules coordinate with Na, where the Na–O distances are 2.48 and 2.32 Å. Analcime can be found in a range of compositions, from $NaAlSi_3O_8{\cdot}1.5(H_2O)$ to $NaAlSi_{1.5}O_5{\cdot}0.5(H_2O)$ [10]; and in some cases, K can substitute for Na [11].

Many Raman spectroscopic studies of silicate glasses (e.g., [12–16]) present vibrational assignments to spectral features in the context of various glass composition series, comparisons between compositionally similar crystalline and amorphous silicates, and calculated Raman spectral features from hypothetical silicate glass structural units. The Raman spectra of these glasses are dominated by broad bands or envelopes of overlapping bands, that are mostly due to vibrational modes within polymerized networks comprised mainly of linked silicate tetrahedra (SiO_4). Higher frequency features are assigned to more localized atomic displacements within these networks.

Silicate glass Raman spectra contain a broad, highly polarized envelope (Fig. 3), at frequencies below 650 cm^{-1}, that is assigned to O–Si–O and Si–O–Si bending modes, as well as longer-range atom displacements within rings of linked tetrahedra. Bridging-oxygen breathing modes, between linked silicate tetrahedra within various membered rings, have been assigned to relatively narrow features between 400 and 700 cm^{-1}; smaller Si–O–Si angle bending modes typically within smaller rings are assigned to higher frequency features. For amorphous SiO_2, bridging-oxygen breathing motions in planar four- and three-membered silicate rings have been assigned to the relatively narrow D_1 and D_2 "defect modes" found near 495 and 606 cm^{-1}, respectively [17].

An envelope of bands is observed near 1000 cm^{-1}, that is due to localized Si–O stretch modes within silicate tetrahedra linked to a network by sharing oxygen atoms with other SiO_4, AlO_4, or BO_4 tet-

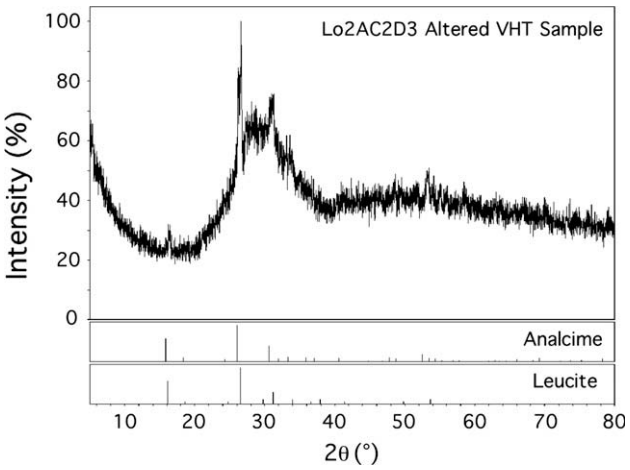

Fig. 1. Representative X-ray diffraction pattern data for an altered VHT sample indicating amorphous (broad features) and crystalline (narrow features) components. Powder pattern histograms of analcime and leucite are plotted below to indicate possible matches with diffraction features in the data.

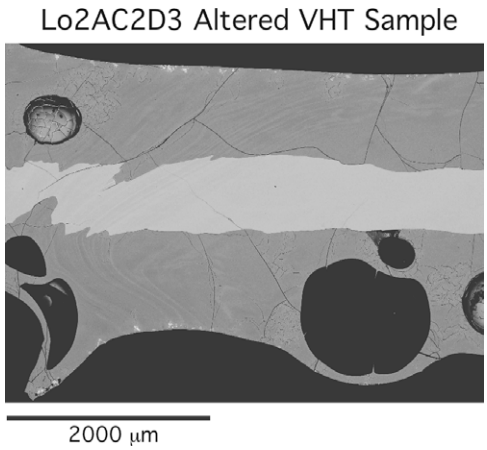

Fig. 2a. SEM backscattered electron micrograph of Lo2AC2D3 altered VHT sample indicating altered glass (darker areas) surrounding remnants of original glass (lighter areas) at the center of the coupon. Note the small crystals near the sample surfaces.

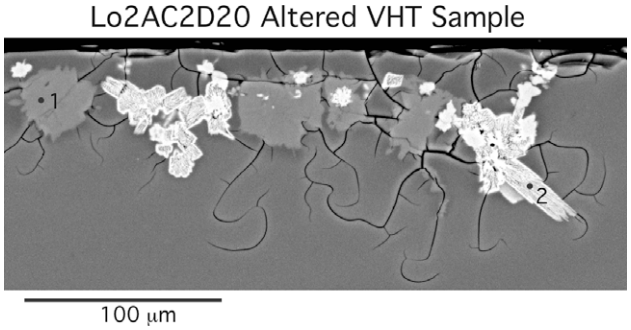

Fig. 2b. SEM backscattered electron micrograph of Lo2A 20 day altered VHT sample indicating a layer of analcime-like crystals (light gray areas: point 1) and leucite-like crystals (bright areas: point 2), as well as surrounding altered glass (gray); SEM–EDS analyses of these two points are listed in Table 1. Some leucite-like crystals are surrounded by analcime-like phases, which may indicate leucite alteration to analcime.

rahedra, or planar BO_3 groups. These bands are assigned to different Q-species in the glass network structure, where, for example, Q^4 is a SiO_4 tetrahedron linked to four other tetrahedra via four bridging-oxygen atoms, and Q^0 is an isolated SiO_4 tetrahedron with no bridging-oxygen atoms. This Si–O stretch envelope has at least four different bands, where each band is assigned to different Q-species tetrahedra [14–16]. In general, as the Q-species become more polymerized, the corresponding Si–O stretch mode has higher frequency. Bands centered near 950, 1040, 1100, and 1140 cm^{-1} can be assigned to Si–O stretch motions within Q^2, $Q^{3'}$, $Q^{3''}$, and Q^4 tetrahedra [15,16]. A $Q^{3'}$ tetrahedron is linked to various combinations of Q^3 and Q^4 tetrahedra, where at least one of the three neighboring tetrahedra is Q^3; in this case, the local network structure can be visualized as silicate tetrahedral sheets, as well as sheets that may be linked to neighboring sheet-like units. $Q^{3''}$ species are linked to three Q^4 tetrahedra, where a local group of tetrahedra may be fully polymerized with the exception of one tetrahedron having a non-bridging oxygen. The Raman spectra of silicate glasses containing hydrous species are shown to have Si–OH stretch modes near 910 cm^{-1} [18].

Higher frequency Raman modes are associated with stretching displacements within BO_3 triangles, OH, or water molecules. Near 1450 cm^{-1}, a weak intensity broad band is assigned to B–O stretch modes within BO_3 triangles [19]. At frequencies higher than

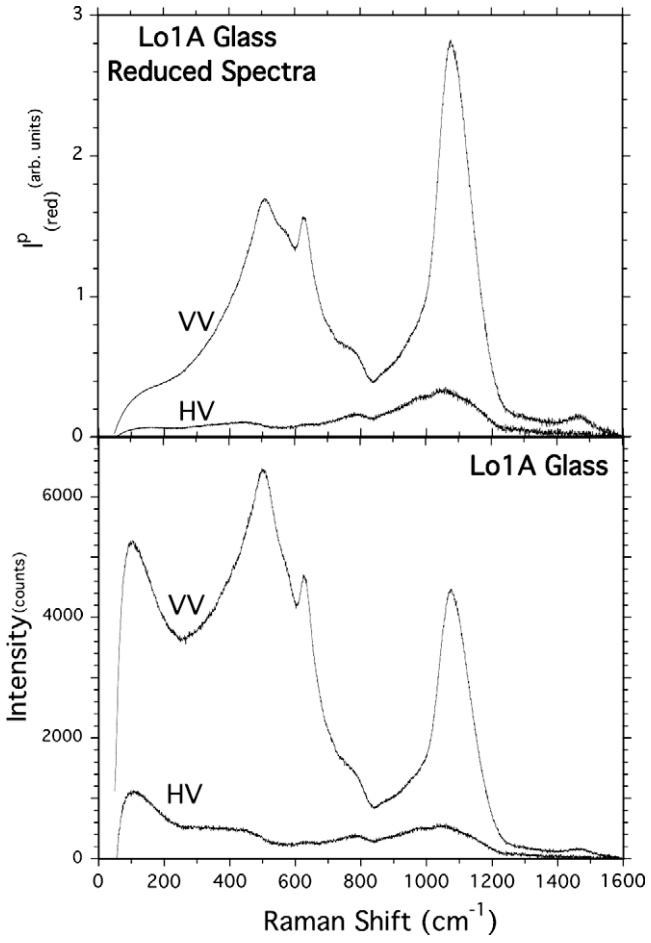

Fig. 3. Polarized Raman spectra of Lo1A glass (bottom plots) and the equivalent reduced Raman spectra (top plots).

1500 cm^{-1}, relatively narrow peaks to enormously broad bands or groups of bands (some with widths over 2000 cm^{-1}) are observed for hydrated glasses and are caused by OH stretch motions, as well as bending and stretching modes within water molecules [15,16,20,21].

1.3. X-ray absorption spectroscopy

Na, Al, and Si each have distinct structural roles in silicate glasses; and XAS data were gathered on the samples of interest for all three elements. Silica-rich glasses consist of a polymerized network dominated by silicate tetrahedra as well as network modifying cations, such as Na. Al can play dual roles in silicate structures: one, being a network former in tetrahedral coordination (AlO_4) linked to other tetrahedra, and two, being a network modifier in octahedral coordination (AlO_6).

An X-ray absorption spectrum can be divided into two regions: the X-ray absorption near-edge structure (XANES) that includes an absorption edge of the element of interest, and the extended X-ray absorption fine structure (EXAFS). Features at the absorption edge are sensitive to the valence of the absorbing atom as well as to single- and multiple-scattering contributions from the atoms surrounding the absorber. Due to these different contributions of features at the absorption edge, obtaining unambiguous information from XANES about the absorbing element can be difficult. However, XANES calculations can provide insights into the causes behind specific XANES features, especially for crystalline samples where an atomic environment is known from crystal structure

determinations. EXAFS data, by convention, are extracted from a spectrum at approximately 20 eV beyond the absorption edge to higher energies. In many cases, EXAFS oscillations are due primarily to single scattering of the spherical electron wave emitted by the absorbing atom from the arrangement of atoms surrounding the absorber. Through fitting procedures, EXAFS data are analyzed to quantitatively determine average bond distance (r (Å)), coordination number (n (atoms)), and degree of disorder (Debye–Waller factor or σ^2 (Å^2)) of shells of atoms around the absorber.

XAS data were collected for three crystalline standards, α-quartz (SiO_2), analcime, and leucite, to model the Na, Al, and Si environments in the borosilicate glasses: Lo1A and Lo2A, and their altered VHT counterparts. Only Al and Si K-edge XANES are presented because the energy ranges scanned for these elements were too narrow to do a full EXAFS analysis. However, the energy range scanned at the Na K-edge was wide enough so that EXAFS analyses could be done.

Earlier studies [22–28] characterized the Na environments in some silicate minerals and glasses using XAS. Na XANES data were presented for a variety of crystalline silicates [22,24,27,28]; calculated Na XANES spectra were also presented for a few silicates [22,24], where qualitative similarities were demonstrated between theory and experiment. Na EXAFS data and analysis results are reported for the local Na environments within a variety of silicate glasses [23,25–27], which generally have average Na–O distances between 2.30 and 2.50 Å with three to five oxygen nearest-neighbors. The results from these studies will be compared with the Na XAS data and analysis findings for the samples investigated here.

Al XANES studies [29–32] show that Al K-edge features are sensitive to Al coordination. Crystals having tetrahedral AlO_4 have a single edge maximum at 1566 eV, while crystal structures with relatively undistorted octahedral AlO_6 (all Al–O distances similar) have two edge maxima near 1568 and 1572 eV. It has been shown for Ca-aluminosilicate glasses [32], that the amplitudes of certain tetrahedral Al XANES features are sensitive to the silica content of the sample; this finding may be used to determine numbers of silicate tetrahedra linked to each AlO_4 tetrahedron within a polymerized network.

Si XANES are presented on a variety of minerals that contain silicate tetrahedra [33], as well as the high pressure phase, stishovite (SiO_2), which has six-coordinated Si [34]. The Si K-edge peak, or white-line, is near 1846.8 eV for minerals containing tetrahedral Si and can shift to higher energies up to 1848.1 eV, where edge features are similar. The edge peak for the SiO_6 environment in stishovite is at 1849.0 eV [34]. Correlations were discovered between the Si K-edge energy and specific structural and chemical characteristics of each mineral. As the SiO_4 tetrahedra become more polymerized in a crystal structure, linking with other SiO_4 and AlO_4 tetrahedra, the edge shifts to lower energy. Edge energy shifts can also be correlated to Al content within similarly polymerized structures, where lower Si K-edge energies are also observed for tetrahedral networks containing more Al.

2. Experimental

2.1. Sample preparation and basic characterization

All samples measured were bulk fragments. Phase identification of the crystalline standards: quartz (NMNH #R17669 from Hot Springs, Arkansas), analcime (NMNH #104655 from County Antrim, Ireland) and leucite (NMNH #167389 from Napoli, Italy), was verified by powder XRD. The Lo1A and Lo2A glasses used for this study were synthesized from reagent grade chemicals [1] and were confirmed to be crystal-free by XRD. The glass fragments were taken from homogeneous portions of the annealed melt material. The VHT samples were subjected to a saturated hydrous atmosphere at 200 °C for 3 days (Lo1AC2D3 and Lo2AC2D3) and 20 days (Lo1AC2D20 and Lo2AC2D20) in 304L stainless steel Parr series 4700 type screw-cap 22 ml pressure bombs [3]. The glasses were cut to approximately 10 × 10 × 2 mm coupons; and the small dimension between the parallel faces was accurately measured to enable calculation of the mass of the reacted glass after the VHT. A 1.6 mm diameter hole was drilled near one edge of the coupon so that the glass sample could be suspended from a hanger made of 24 guage stainless steel. For each altered VHT wafer, cross-sections were cut and then mounted for SEM imaging, measurement of the altered glass, and chemical analyses. The 3-day VHT samples contain some of the as-melted glass in the center of each wafer (Fig. 2a), while the 20-day VHT samples were almost completely altered; all VHT altered samples contain some crystals near the sample surfaces (Figs. 2a and b).

Chemical analyses were performed on the as-melted glass powders by X-ray fluorescence (XRF) techniques and on the altered VHT samples by SEM (Table 1). Compositions of crystalline phases were determined in a JEOL JSM-5910-LV SEM operating at 25 kV accelerating potential and about 0.75 nA using an Oxford INCA Energy 300 EDS system and software in the standardless mode. While the results indicate qualitative agreement with the identification of phases from XRD data as leucite and analcime, the silica content is excessive in both cases (Table 1). This may be due to the inclusion of a significant amount of amorphous silica in the crystal growth area, where micrographs of the crystals suggest a mosaic pattern of growth (Fig. 2b). Chemical analyses of the amorphous portions of the VHT altered sample cross-sections (Figs. 2a and b and Table 1) were performed by SEM using wavelength dispersive spectroscopy (WDS). Original glasses were used as standards for quantitative analyses. The WDS analyses of the modified glass areas were also done in the JSM-5910-LV employing an Oxford Wave 700 system and software. The analyzed unmodified glasses were used as standards. All analytical data were acquired with a beam current of about 35 nA at 10 kV accelerating potential. To minimize the effect of alkali migration on analysis, analytical conditions were kept the same for both standardization and measurement, the alkalis Na and K were measured first, and the beam was rastered over a frame dimension of about 10 × 15 μm on the sample during measurement. The order of measurement was Na, K, Al, Si, and B, with peak dwell times of 20, 20, 10, 10, and 100 s, respectively. Two backgrounds were collected for every element analyzed, each at ½ the peak dwell time. Oxygen was not measured directly, but determined by stoichiometry. Multiple analyses of the unmodified glasses against themselves proved that reliable results could be obtained using the above conditions. Quantitative results for the modified glasses were not normalized; and the average deficit between totals for the unmodified and modified material (between 9 and 3 wt.%) was taken as an indicator of the density change attributable to material loss and water or OH uptake (Table 1). SEM–WDS indicates significant Na_2O depletion and some B_2O_3 enrichment in the VHT altered samples with respect to their as-melted glasses (Table 1).

Alteration rates during the VHT were determined for the glasses investigated by measuring the total thickness of the altered layers for samples subjected to 1–3 and 20 day VHT. For shorter duration VHT altered samples (up to 3 days), all rates were similar and averaged to 638.8 g/m^2/day. However, the rate slowed considerably to 139.7 g/m^2/day comparing alteration thicknesses from the 3 to 20 day samples. This slower rate is due to the sample running out of glass to be modified. As a result, in the 20 day samples, almost all of the coupon had been altered.

XRD and SEM–EDS also indicate (Figs. 1, 2a and b) that the VHT samples investigated contain minor amounts of Na-rich

equi-dimensional analcime-like crystals and K-rich elongated leucite-like crystals within 200 μm of the sample surface in an amorphous matrix. Both crystalline phases are in close proximity with each other, where some of the smaller leucite-like aggregates are inter-grown with or completely surrounded by analcime-like phases.

2.2. Raman spectroscopy

A single grating spectrograph – notch filter micro-Raman system [35] was used to gather the Raman spectra presented here. An EXCEL Model 3000 Ar^+ laser provided the 5145 Å wavelength incident light that was directed through a broad band polarization rotator (Newport Model PR-550) to the laser microscope which guided the laser light down to the sample surface through a long working distance Mitutoyo 10× microscope objective. The laser light was focused to a 10 μm diameter spot on each sample. The laser light power was approximately 25 mW at the sample. Room temperature polarized spectra were gathered in back-scattering geometry. The scattered light was directed through an analyzer polarizer in the microscope column that was set to one orientation for all polarized spectra collected. After the analyzer, the scattered light proceeded through holographic notch and super-notch filters (Kaiser Optical Systems), which reduced the Rayleigh scattered light intensity by 10 optical densities. The notch filters were oriented in the scattered light path so that the filter cut-off frequency was minimized to near 70 cm^{-1} from the laser line. The spectrograph used a 300 and a 1200 gr/mm grating (Richardson Grating Laboratory) that was set to disperse the Stokes scattered light from the sample onto a 2048 × 512 element Peltier cooled CCD detector (Model DU440BV, Andor Technology). Due to the relatively broad spectral features for most of these samples, the incident slits of the JY-Horiba HR460 spectrograph were set to 18 cm^{-1} resolution for the 300 gr/mm grating and to 6 cm^{-1} resolution for the 1200 gr/mm grating to collect spectra from 50 to 4500 cm^{-1} and from 50 to 1600 cm^{-1}, respectively. The spectrograph was frequency calibrated using CCl_4, so that the recorded frequencies are accurate to within ±1 cm^{-1}. Parallel-polarized (VV) or cross-polarized (HV) spectra were collected, where the incident laser light was vertically or horizontally polarized, respectively, as it entered the microscope. Each spectrum is an average of 10 exposures, collected at 10 s each. All spectra were corrected for notch filter, grating efficiency, and detector quantum efficiency effects on the scattered light intensities (Figs. 3–5).

Two inter-related problems arise when comparing the Raman spectra of the original glasses with the altered VHT samples investigated: Rayleigh scattering differences and color differences. The altered VHT samples are translucent white to gray-brown, compared with the original glasses, which are clear and colorless. The darker color VHT samples cause more Rayleigh scattering, producing a more intense "Rayleigh tail" at frequencies under 200 cm^{-1} than the original glasses (Fig. 5, top three plots). Compared with the original glasses, the darker VHT samples also absorb more of the incident laser light, which reduces the sample volume producing the Raman signal.

2.3. X-ray absorption spectroscopy

The XAS data were collected under vacuum at Beam Line 6.3.2 at the Advanced Light Source (ALS), Lawrence Berkeley National Laboratory (LBNL). The average synchrotron running conditions were from 380 to 200 mA at 1.9 GeV. The spectra were gathered so that the variable line spacing plane grating monochromator was scanned through a 300 eV energy range, where each scan included the Na, Al, or Si K-absorption edge; the energy resolution is approximately 1 eV for these data. Fluorescence spectra were gathered, where the incident (I_0), and backscattered fluorescence

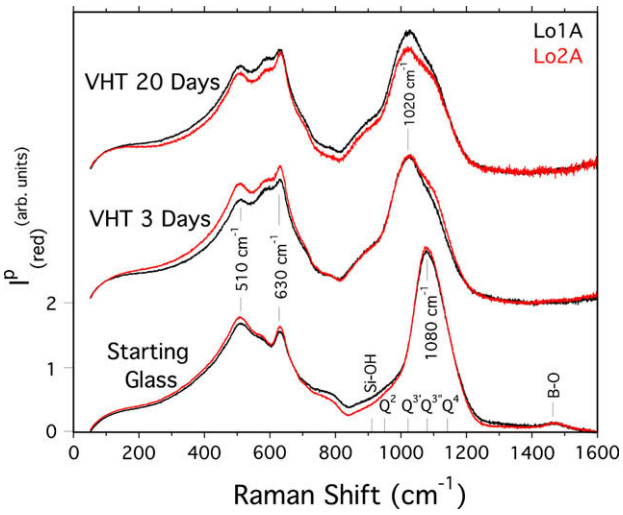

Fig. 4a. VV polarized reduced Raman spectra of the as-melted glass and the two corresponding VHT altered coupons: Lo1A samples (black line) and equivalent Lo2A samples (red line). Some band frequencies and vibrational assignments are indicated. Spectra are offset for clarity. (For interpretation of the references to colour in this figure legend, the reader is referred to the web version of this article.)

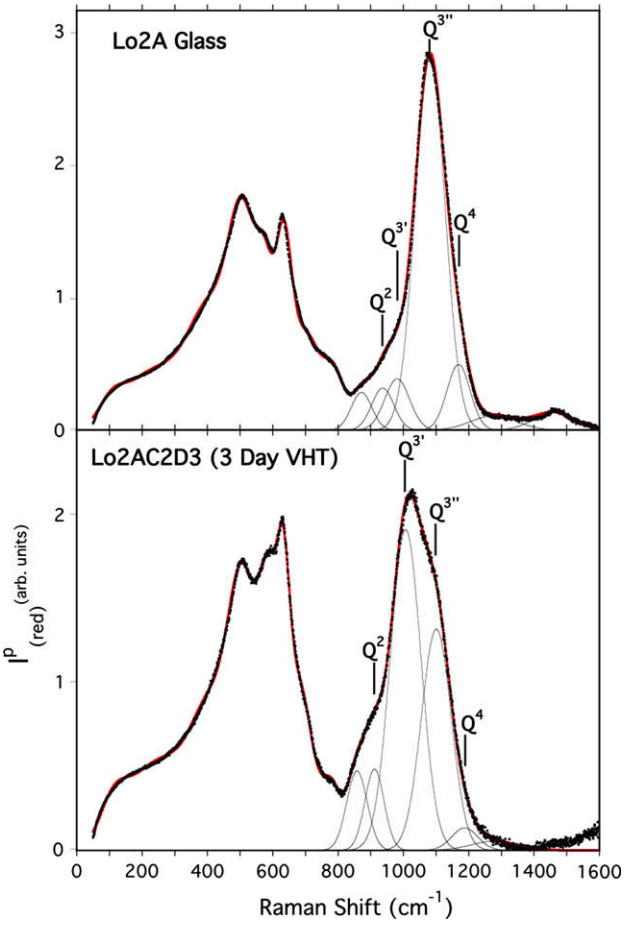

Fig. 4b. Reduced Raman spectra Gaussian fitting of the high frequency envelope to determine Q-species abundances in Lo2A glass and the corresponding Lo2AC2D3 altered sample. Data plotted as black points, fit Gaussian peak components plotted as black lines with corresponding Q-species labels, and sum of the fit plotted as a red line. (For interpretation of the references to colour in this figure legend, the reader is referred to the web version of this article.)

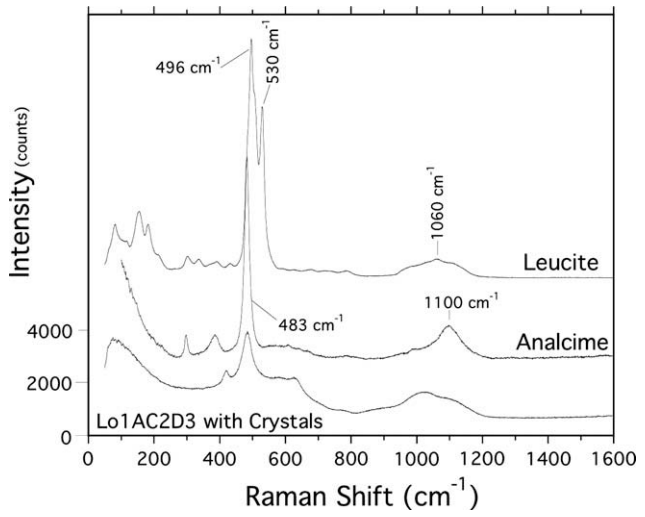

Fig. 4c. VV polarized Raman spectra of polycrystalline leucite and analcime, as well as a point in Lo1AC2D3 containing crystals. Frequencies of some of the more prominent features are indicated. Spectra are offset for clarity.

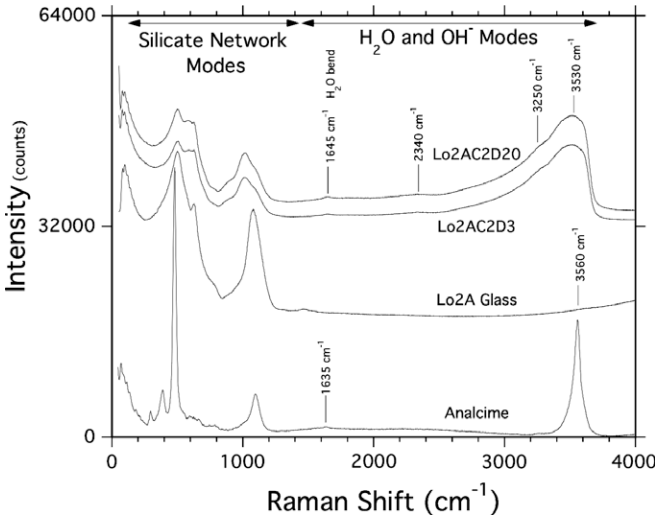

Fig. 5. VV polarized Raman spectra of analcime, Lo2A glass, and the two Lo2A VHT samples including the water and OH mode frequency range. Vibrational modes and frequencies of some of the more prominent features are indicated. Spectra are offset for clarity.

(I_f) X-ray intensities were each measured using a channeltron. The flat sample surface was positioned nearly perpendicular with respect to the incident beam. Ideally, each XAS spectrum collected is the absorption coefficient (μ) of the sample versus energy, where μ is proportional to I_f/I_0. Acquiring fluorescence XAS data free of self-absorption distortions depends on preparing sample thicknesses on the order of one absorption length of the material of interest. Gathering distortion-free XAS data for the low energy K-edges for Na, Al, and Si, require such extremely thin samples, that surface effects would dominate the structural contributions to the XANES and EXAFS. To avoid this problem, bulk samples were used; and the resulting XAS data were corrected for thickness effects (see Section 4). The Na, Al, or Si K-edge fluorescence spectrum of analcime was taken periodically for energy calibration purposes to eliminate any energy drift over time in the data due to the monochromator. There is no evidence that VHT sample dehydration took place under vacuum, because there was no out-gassing from these samples during the sample chamber pump-down, and because both vacuum exposed and unexposed portions of the these samples have nearly identical Raman spectra.

2.4. Thermogravimetric analyses

To determine the amount (wt.%) of hydrous species incorporated into Lo2A glass during the VHT, thermogravimetric (TG) analyses were performed on Lo2AC2D20 in a SETARAM MHTC96 high temperature calorimeter using the TG-differential scanning calorimeter (DSC) module. The mass of the sample and the heat flow between the sample and reference were monitored in a He atmosphere while the temperature of the sample was increased. The temperature program consisted of a first ramp from room temperature to 130 °C, which drove off any surface water, and a second ramp (run at 5 °C/min) from 130 °C to 800 °C, to drive off structural water and OH.

3. Raman data processing

In an attempt to quantify changes in the areas of the Si–O stretch bands near 1000 cm^{-1}, the spectra of the original glasses and altered VHT samples were reduced (Fig. 3) so that all Raman intensities are equally weighted throughout each spectrum [14,36,37]. The reduced VV spectra were then fit by a series of Gaussian peaks to determine areas of the Si–O stretch modes associated with various Q-species tetrahedra, as summarized earlier. However, the magnitudes of the total Raman intensity for each glass versus that for the corresponding VHT samples were different due to the sample color-translucency differences. Since the compositions of these samples are similar (excluding water or OH content, see Table 1) it is assumed that the total area of all Raman features below 1400 cm^{-1} is the same among all glass and VHT altered samples investigated. Rescaling each VHT altered sample spectrum was done so that the total area fit to those spectral features was the same as that fit to the original glass spectra (Fig. 4b).

Several fitting routines for the Si–O stretch mode envelope were attempted that constrained Gaussian peak centroid frequencies to the 950, 1020, 1080, 1140 cm^{-1} values determined by Zotov and Keppler [15,16] for the Q^2, $Q^{3'}$, $Q^{3''}$, and Q^4 Si–O stretch bands, respectively, in the Raman spectra of Na-tetrasilicate glasses. However, routines that used these centroid frequencies could not completely fit the Raman spectra (Figs. 4a and b), which is likely due to the greater variety of vibrational environments in the samples investigated here compared with those in Na-tetrasilicate glasses [15,16]. Zotov and Keppler could make quantitative correlations for their Na-silicate glass system between specific Q-species Raman features and their Si NMR results. In the samples investigated here, SiO_4 tetrahedra can share oxygen atoms with many combinations of SiO_4, AlO_4, and BO_4 tetrahedra, as well as BO_3 triangles, and can also have non-bridging oxygen atoms bonded to Na^+ or K^+ network modifiers. Each one of these environments, that include atoms other than Na, Si, and oxygen, probably have Si–O stretch Q-species modes that are frequency shifted with respect to the corresponding modes determined for the Na-tetrasilicate glasses [15,16]. The Raman scattering cross-sections (intensities) of the Si–O stretch modes for the samples investigated here are also likely to have some differences with respect to those for the Na-tetrasilicate glasses due to the chemical differences.

Other routines using common Gaussian peak centroid frequencies for original glass and VHT sample spectra were tried. Unfortunately, these fitting routines could not converge for all spectra analyzed here. Peak centroid frequencies needed to be varied up to 26 cm^{-1} so that peaks centered at 937, 981, 1081, and 1170 cm^{-1} were fit to the original glass spectra, while corresponding peaks centered at 912, 1007, 1101, and 1188 cm^{-1} were fit to the VHT sam-

ple spectra (Fig. 4b, bottom). From low to high frequencies, these four peaks could then be assigned to the Q^2, $Q^{3'}$, $Q^{3''}$, and Q^4 Si–O stretch modes defined earlier [15,16]. The choice of the Si–O stretch mode assignments to the Gaussian peaks presented above is a simple (and possibly, over-simplified) assignment scheme that can be determined for the data presented here, out of many other ways of fitting Gaussian peaks, that result in statistically equivalent deviations between the fit and the reduced Raman spectrum. Due to the differences between the more chemically complex samples investigated here and the Na-tetrasilicate glasses investigated elsewhere [15,16], the fitting routine used here provides only an approximate determination of the Q-species changes between the original glasses and the corresponding altered VHT samples.

4. XAS data analysis

The XANES fluorescence spectra were initially processed using standard pre-edge background subtraction and edge-step normalization procedures [38]. By using bulk samples with relatively large Na, Al, and Si concentrations, significant self-absorption effects damp features near the edge in each spectrum. Therefore, the XANES spectra were corrected for self-absorption by the program FLUO [39]. After normalization and calibration, direct comparisons can be made with XANES data for all samples to an energy accuracy of ±0.1 eV (Figs. 6a–e).

Na K-edge calculations for analcime were performed using FEFF8 [40] to better understand the changes in Na XANES features observed for the samples investigated. The calculations generally followed the procedure outlined by Neuville et al. [22,41], where a Hedin–Lundqvist type exchange potential was used, and the self-consistent potential calculation used a maximum cluster radius of 4.8 Å, while the full multiple-scattering part of the calculation used a maximum radius of 8.0 Å. The calculation that best matched the experimental data used the $Z+1$ model [32,41,42], where Mg, instead of Na, was placed at the origin of the cluster, which simulates the excited electronic configuration of the photo-absorber by promoting the core electron to a valence orbital. As observed earlier [22], this model significantly increased the calculated amplitude of the edge feature near 1076.7 eV compared with that using Na at the cluster's origin.

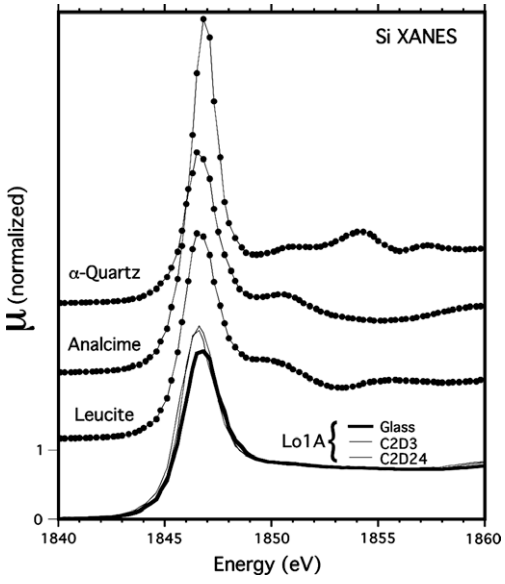

Fig. 6a. Si XANES spectra of the three standards (points and line), as well as the Lo1A glass (thick line) and corresponding VHT samples (thin lines). Si XANES for the Lo2A samples follow the same trend as that presented here for the Lo1A samples. All spectra indicate tetrahedral Si coordinated to four oxygen atoms. Plots are offset for clarity.

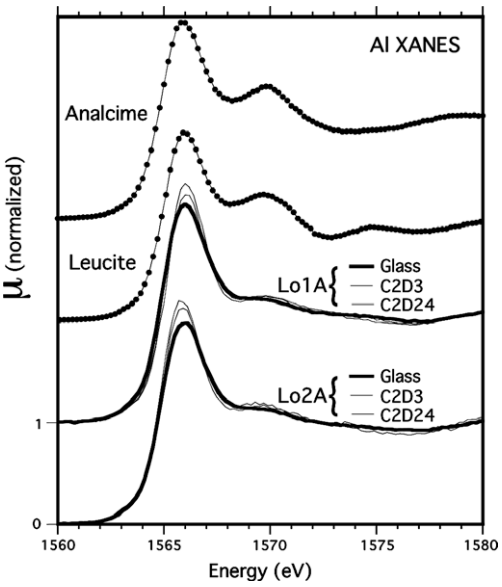

Fig. 6b. Al XANES spectra for the analcime and leucite standards (points and line), as well as the Lo1A and Lo2A glasses (thick lines) and VHT altered samples (thin lines). All spectra indicate tetrahedral Al coordinated to four oxygen atoms. Plots are offset for clarity.

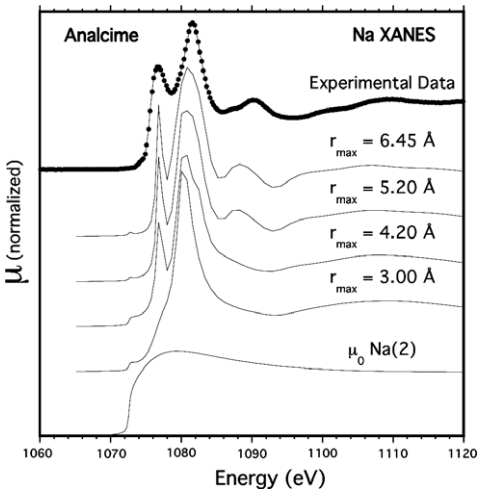

Fig. 6c. Na XANES data for the crystalline standard analcime (top: points and line) and XANES calculations for various diameter atom clusters around the Na(2)-site: from μ_0 (atomic Na contribution only) to r_{max} = 3.00 Å (nearest-neighbor two H_2O and four oxygen atoms) to r_{max} = 6.45 Å (87 surrounding atoms).

Na EXAFS data for the samples measured also contain self-absorption effects that were corrected by the program SABCOR [43]. For most samples, four spectra were collected, where two data sets were averaged together to produce two spectra for analysis. A cubic spline function was fit to and then subtracted from the edge-step normalized data ranging from near 10 to 230 eV above E_0. Energy values in eV were converted to k (Å^{-1}) [38], where the resulting $\chi(k)$ data were k^3-weighted (Figs. 7a and b). The $k^3\chi(k)$ data were then Fourier-transformed over the $2.0 < k < 7.7$ Å^{-1} range, using a Hanning window of 1.0 Å^{-1} on the upper and lower limits of the data to minimize Fourier-transform termination artifacts in the resulting partial radial distribution function (RDF). Peaks in the RDFs correspond to shells of atoms surrounding Na

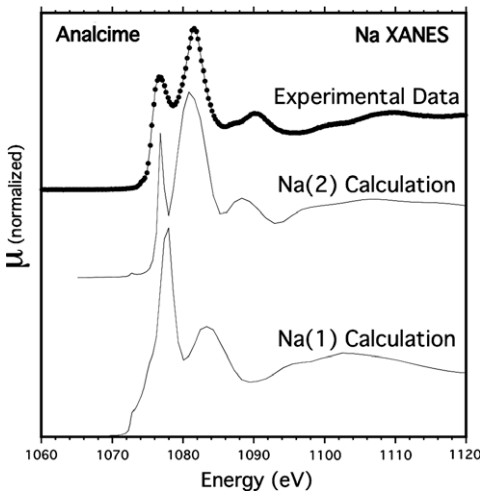

Fig. 6d. Na XANES data for analcime (points and line) and FEFF8 XANES calculations for the Na(1) and Na(2)-sites in the analcime crystal structure (line only).

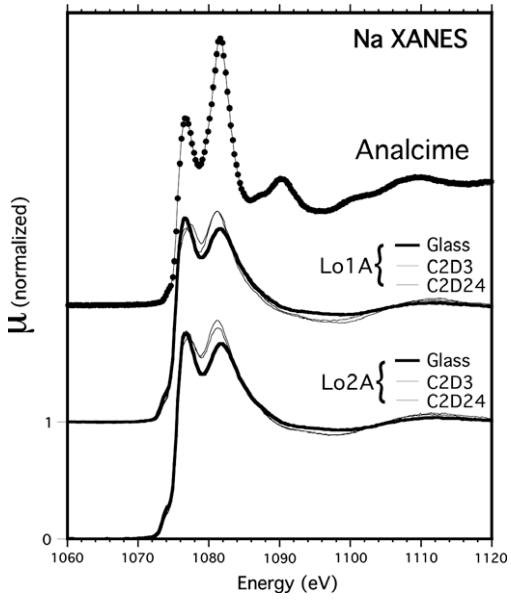

Fig. 6e. Na XANES spectra for analcime (points and line) and the Lo1A and Lo2A glasses (thick lines) and VHT altered samples (thin lines). Plots are offset for clarity.

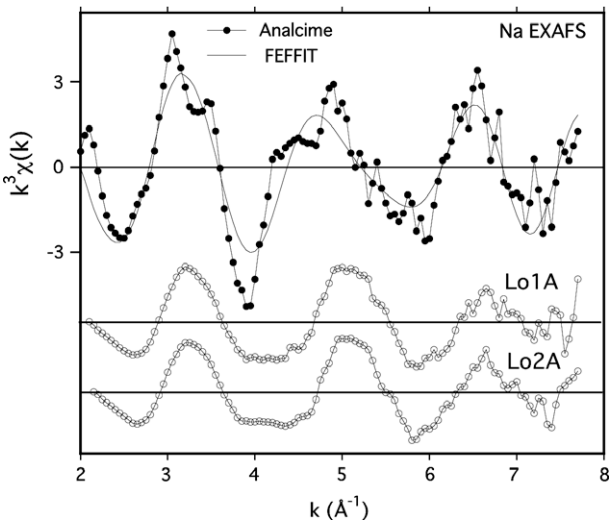

Fig. 7a. Na EXAFS $k^3\chi(k)$ data (points and line) and fit (line) for the analcime crystalline standard (top) and data for the two glasses investigated (bottom plots: line and open points). Plots are offset for clarity.

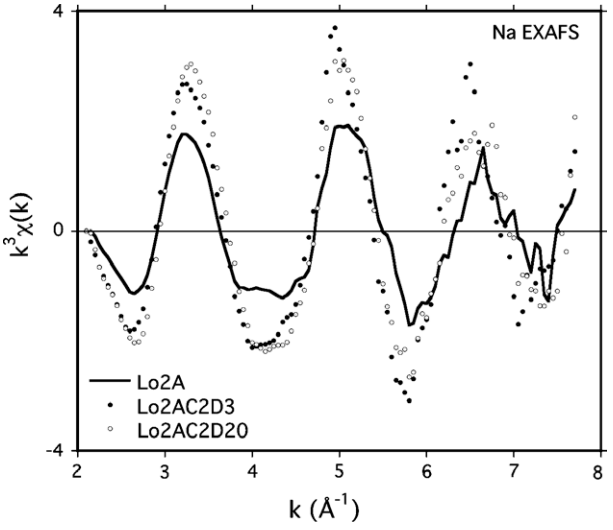

Fig. 7b. Na EXAFS $k^3\chi(k)$ data for the Lo2A glass (line) and VHT altered samples (points): Lo2AC2D3 and Lo2AC2D20 for 3 and 20 days, respectively.

(Figs. 8a and b), where r, n, and σ^2 for each shell can be obtained from the fitting procedure, FEFFIT [44] (Fig. 9a and b). The position of each peak in the RDF is phase-shifted to lower r by approximately 0.3–0.5 Å with respect to the actual average bond distance that corresponds to each peak. The RDF fitting range for the analcime standard was from 1.1 to 3.2 Å that included the first- and second-nearest-neighbor peaks at 1.9 and 2.8 Å, respectively. The RDF fitting range for the glasses and corresponding VHT samples was from 1.10 to 2.45 Å, which included the nearest-neighbor peak. For EXAFS analysis, atom clusters, surrounding a central Na to a maximum radial distance of 4 Å, were generated to simulate the analcime structure [8]. These clusters were used by FEFF7.02 [44] to calculate the theoretical EXAFS for analcime. By taking into account the important atom correlations calculated by FEFF from the analcime structure, Na–O and Na–Si path contributions could then be used to label major peaks in the analcime RDF (Fig. 8a).

The analcime structure can be variable in samples from different localities [8,10]. The most likely structure of the sample used here has tetragonal symmetry and contains Na(1)- and Na(2)-sites, where Na has some positional uncertainty [8]. The local environments of these two sites have six oxygen atoms (including those associated with water), have pseudo-octahedral symmetry, but are different, especially with regard to structural H_2O molecules. For Na(1), all six oxygen atoms, including two associated with H_2O molecules, have Na–O distances within 0.02 Å of 2.48 Å. However, the Na(2)-site has more distortion from octahedral symmetry compared with Na(1), and includes two H_2O molecules at 2.32 Å, and four other oxygens at 2.55 Å from Na. Both Na-sites have linear H_2O–Na–H_2O arrangements with similar atom distributions beyond the nearest-neighbor oxygen atoms and H_2O molecules.

Analcime was the Na EXAFS standard used for the first-shell RDF peak fitting. The dominant contributions to the theoretical X-ray absorption spectrum for analcime are the Na–O nearest-

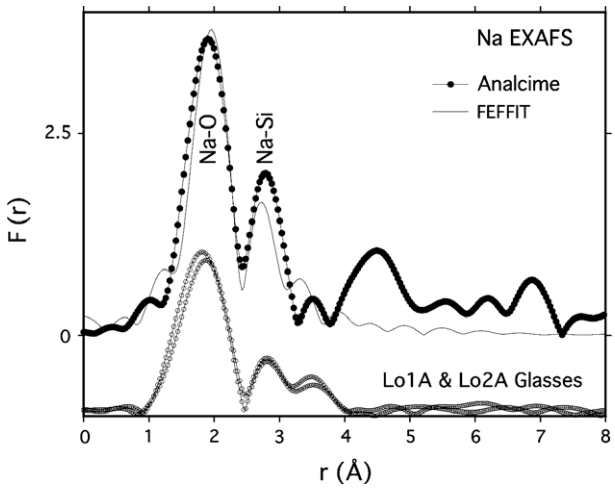

Fig. 8a. Na EXAFS partial RDF data (points and line) and fit (line) of the analcime standard (top plots) and the two glasses investigated (lower plots: line and open points). For analcime, pair correlations assigned to the major nearest-neighbor RDF peaks are indicated. Plots are offset for clarity.

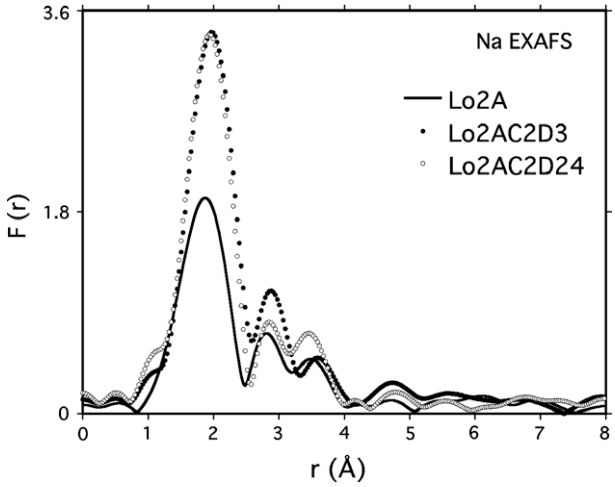

Fig. 8b. Na EXAFS partial RDF data for the Lo2A glass (line) and VHT altered samples (points).

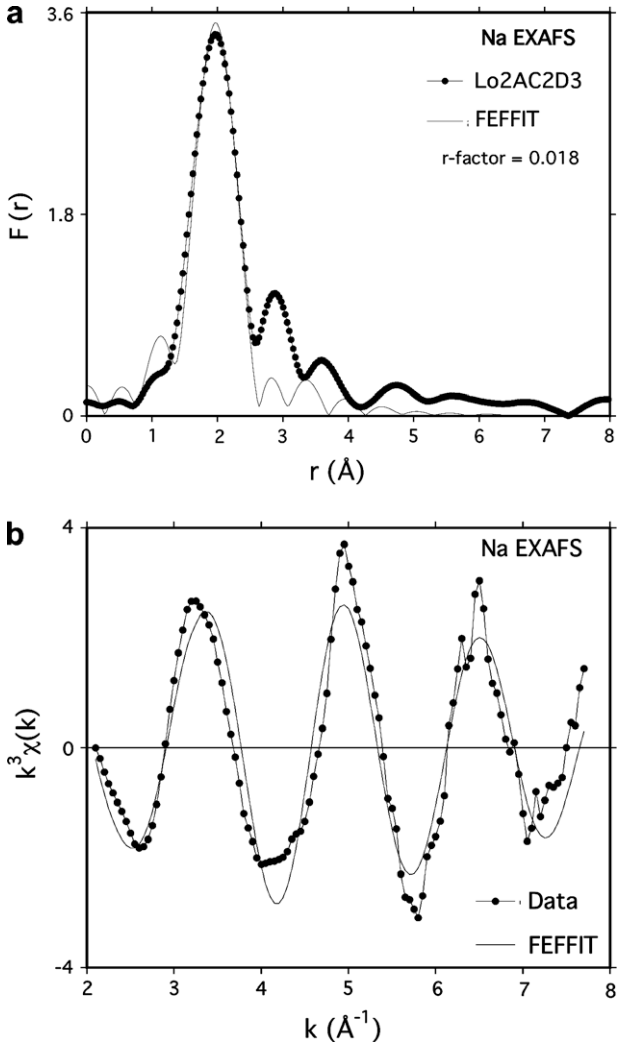

Fig. 9. Na EXAFS fitting for Lo2AC2D3 VHT altered sample: (a) partial RDF and (b) $k^3\chi(k)$ data. Final fitting parameters listed in Table 2.

neighbor single scattering paths. The 2.47 Å Na(1)–O path and the 3.14 Å Na(1)–Si path were used by FEFFIT to fit the first-shell peak near 1.9 Å and a second-shell peak near 2.8 Å, respectively, in the RDF (Fig. 8a) by initially holding r and n to the known values for this structure, while varying E_0, s_0^2 (a scaling factor that includes EXAFS amplitude damping effects [38]), and σ^2 for each path. An E_0 of 1078.7 eV (ΔE = 5.0 eV) and an s_0^2 of 1.00, were determined for the initial fits of the analcime data, where reasonable σ^2 values were obtained. The s_0^2 and E_0 parameters were then constrained at the above values, while r, n, and σ^2 were varied. The Na–Si coordination number was constrained to 2.0 for the fit to converge (Table 2).

The first-shell RDF peaks for the glasses and corresponding VHT samples were fit by varying r, n, and σ^2 for the 2.47 Å Na–O analcime path (e.g., Fig. 9a and b). The EXAFS fitting routines for the Lo1A and Lo2A glasses needed to vary ΔE_0 from the analcime procedure to improve the overall fit and minimize the uncertainties determined by FEFFIT. For all glasses and VHT samples, averages for r, n, and σ^2, as well as their uncertainties are listed in Table 2.

5. Discussion

5.1. Raman spectroscopy

5.1.1. Analcime and leucite standards

The Raman spectra for polycrystalline fragments of each phase (Fig. 4c) are similar to data presented elsewhere for these minerals [13,45]. The spectra are dominated by T–O–T (where T = Si or Al) bending modes near 500 cm^{-1} [13]. The leucite spectrum has two main peaks near 496 and 530 cm^{-1}, which differ from the prominent 483 cm^{-1} peak for analcime. The higher frequency Si–O stretch modes are also different between these two phases, where leucite has weak modes centered near 1060 cm^{-1}, while analcime has a more prominent peak near 1100 cm^{-1}. The analcime spectrum also contains peaks near 1635 and 3560 cm^{-1} (Fig. 5, bottom) that are similar to Raman-active OH and water modes for other zeolites [46].

5.1.2. Lo1A and Lo2A glasses

The spectra for both Lo1A and Lo2A glasses are nearly identical and show a polymerized network structure that has a distribution of Si–O–Si angles, dominated by Q^3 species with some Q^4 tetrahedra, and small amounts of Q^2 tetrahedra (Figs. 3, 4a, b, and 5 (middle plot)). A broad, weak intensity band near 1460 cm^{-1} indicates

Table 2
Na-EXAFS first-shell Na–O fitting results for the analcime standard, glasses, and altered glasses investigated using $s_0^2 = 1.00$. *constrained fitting parameter. Uncertainties are listed in parentheses.

Sample	r-factor	E_0 (eV)	r (Å)	n (atoms)	σ^2 (Å^2)
Analcime Na–O					
EXAFS	0.084	5.0	2.44 (0.02)	7.2 (3.8)	0.0180 (0.0104)
Actual [8]			2.47	6.0	
Na–Si					
EXAFS			3.09 (0.04)	2.0*	0.0067 (0.0058)
Actual [8]			3.17	2.0	
Lo1A glass	0.022	−3.9	2.27 (0.01)	4.4 (1.1)	0.0181 (0.0046)
Lo1AC2D20 altered	0.046	5.0	2.37 (0.01)	4.8 (1.6)	0.0129 (0.0057)
Lo2A glass	0.025	0.5	2.31 (0.01)	3.1 (0.8)	0.0138 (0.0041)
Lo2AC2D3 altered	0.016	5.0	2.38 (0.01)	4.3 (0.8)	0.0105 (0.0032)
Lo2AC2D20 altered	0.013	5.0	2.36 (0.01)	5.3 (1.0)	0.0149 (0.0032)

B–O stretch modes from BO_3 triangles. Since these spectra are similar, the addition of K_2O at the expense of Na_2O in Lo2A glass with respect to Lo1A glass, has little to no effect on the borosilicate network. There is also no evidence of hydrous species in these glasses, because no Raman features are observed at frequencies greater than 1500 cm^{-1} (Fig. 5), except for an increasing luminescence background starting near 3500 cm^{-1}.

5.1.3. VHT altered samples

Raman spectra from the amorphous parts of all VHT samples investigated are nearly identical and show that alteration of the original glass structure was basically completed after 3 days of hydrothermal exposure for both glass types (Fig. 4a). Differences in the Raman spectra between the original glasses and amorphous portions of the VHT altered samples indicate partial depolymerization of the silicate network (Figs. 4a and b). The relative intensities of the 510 and 630 cm^{-1} peaks are reversed, which may indicate larger populations of smaller-membered silicate tetrahedral rings (such as more three-membered rings and fewer four-membered rings) in the VHT samples compared with the original glasses. Si–O stretch envelope peak fitting results for the VHT altered samples versus the original glasses show an area increase of nearly 25% for the Q^2 band, a more than fivefold area increase for the $Q^{3'}$ band, a 50% area decrease for the $Q^{3''}$ band, and a 70% area decrease for the Q^4 band. Increased intensity near 900 cm^{-1} in the spectra for all VHT altered samples with respect to the original glass spectra, can be attributed to Si–OH stretch modes from OH incorporation into the VHT altered glass structure [18].

These network depolymerization results for the VHT process are different with respect to observations presented in studies about alteration of glass powders, that show leached layers with increased silicate tetrahedral polymerization compared with the original glass [4,7]. These variations in leaching behavior of the glass structure may be caused by significant differences in the experimental conditions among our study here and those investigations elsewhere [4,7]. One important factor may be the different starting glass chemistries, where the powders studied [4] contain considerably more B than Lo1A and Lo2A glass coupons. Other factors include: different glass surface to volume ratios, which would be much larger for the powder samples versus the glass coupons used here; different solutions were used: solutions having a pH of 8.5 were used in the powder studies, while distilled water vapor was used here; and different temperatures were maintained during the VHT experiments: 90 °C for the powder studies versus 200 °C for the glass coupons used here.

Raman spectra were also collected at various points near the VHT sample surface that had isolated equi-dimensional crystals, clusters of elongated crystals, or equi-dimensional crystals surrounded by elongated crystals (Fig. 2b). SEM–EDS shows that the equi-dimensional crystals have analcime-like compositions, while the brightly back-scattering elongated crystals have compositions closer to leucite (Table 1, last two rows). The Raman spectra from these points show superposition of broad features from the amorphous matrix and relatively narrow peaks that appear to be from analcime-like and leucite-like phases. For most points measured that contain crystals within Lo1AC2D3, LoA1C2D20, and Lo2AC2D3, a prominent narrow peak is observed near 483 cm^{-1}, which is usually accompanied by enhanced intensity near 1100 cm^{-1} (Fig. 4c, bottom); these features indicate analcime-like phases at these points. For the K_2O-rich Lo2AC2D20 sample, narrow peaks near 516 and 1063 cm^{-1} indicate leucite-like crystals. An intense peak can be also observed near 497 cm^{-1} for some crystals in Lo1AC2D3 and Lo2AC2D3, which also indicate leucite-like crystals. Even the K_2O-poor Lo1A VHT samples have some leucite-like phases. Some crystalline points have prominent Raman modes at frequencies between the strongest peaks for analcime and leucite, which may indicate phases having intermediate compositions between analcime and leucite, as shown by SEM–EDS (Table 1). This solid solution-type behavior is also seen in synthetic samples, where K can replace Na to form K-analcime ($KAlSi_2O_6{\cdot}H_2O$) [10,11].

During the VHT, analcime-like crystals may have formed in two ways. Some analcime-like crystals may have crystallized directly from the glass, as seen in other silicate glasses [5,10]. Other analcime-like crystals may have formed as VHT alteration products of leucite-like phases that crystallized earlier. Analcime-like phases may have crystallized directly from the Lo glasses during the VHT, by considering that synthesis studies [11] show albite + H_2O → analcime + quartz, and that the Lo1A and Lo2A glasses have compositions somewhat similar to albite ($NaAlSi_3O_8$), but with higher Na concentrations and B replacing some Al, where Lo1A glass composition can be written as: $Na_{1.8}K_{004}Al_{0.3}B_{0.7}Si_{2.85}O_8$. SEM images and SEM–EDS also indicate that the crystals observed in the VHT altered samples are possibly inter-grown with amorphous silica, indicating that the above reaction [11] may have taken place. Both Raman and SEM–EDS evidence also show that some leucite-like crystals may be altering to analcime-like phases in the VHT samples (Fig. 2b); this is consistent with studies [45,47] that show three factors are needed to promote leucite alteration to analcime: water (from the hydrated atmosphere), Na^+ (from the original glass), and time (3–20 days).

The weak 1465 cm^{-1} B–O stretch band observed in the Lo1A and Lo2A glass VV spectra, probably disappears under the broad continuum of OH – water modes at higher frequencies in the spectra for the VHT altered samples (Figs. 4a and b, bottom and Fig. 5, top two plots). As a result, analyses of boron-associated bands were not attempted for the VHT altered sample spectra. According to SEM–WDS, boron concentrations for the amorphous VHT phases are higher by approximately 20% than those measured for the original glasses; this indicates that the 1465 cm^{-1} mode is probably present in the VHT spectra.

At frequencies greater than 1600 cm^{-1}, differences are seen among the spectra of analcime, the as-melted glasses, and the amorphous portions of the VHT samples (Fig. 5). Analcime has two relatively narrow peaks at 1635 and 3560 cm^{-1} that can be assigned to modes associated with water. The weak H_2O bending mode near 1645 cm^{-1} [12,15,16] is observed for all VHT altered samples. In the VHT sample spectra, a continuum of broad bands associated with hydrous species has a maximum near 3530 cm^{-1}, that is absent in the original glass spectra. Other components that are part of this continuum are near 3250 and 2340 cm^{-1}. These features are also seen in the Raman spectra of Na-silicate and granitic composition glasses containing at least 2.6 wt.% water

[12,15,16,20]. The relative intensities of silicate network modes (below 1600 cm^{-1}) and hydrous species modes (above 1600 cm^{-1}) in Fig. 5 can be compared with equivalent features in the Raman spectra of Na-tetrasilicate glasses containing various water concentrations [16]; the VHT sample spectra show similarities with the spectra for Na-tetrasilicate glasses containing 5.9–10.0 wt.% water [15,16]. Zotov and Keppler [16] mention that, "All spectroscopic results presented here were obtained on hydrous sodium tetrasilicate glass and as such are not directly applicable to the more complex aluminosilicate systems." The VHT samples investigated here are more chemically complex than Na-tetrasilicate glasses.

However, SEM (Table 1) and DSC analyses of the VHT samples indicate that the above water content estimation from the Raman spectra may be reasonable. SEM–WDS shows that VHT sample composition totals fall short of 100 wt.% by approximately 3–9 wt.%; and this difference is likely due to hydrous species. A DSC run from 40 to 800 °C on Lo2AC2D20 showed two mass loss events: one, a 5.2 wt.% loss from 25 to 130 °C that is due to the liberation of surface hydrous species, and two, a 9.7 wt.% mass loss from 130 to 800 °C, that is due to structural water being released. To check if any hydrous species Raman modes are due to surface water or OH, the first mass loss DSC event was simulated by holding a Lo2AC2D20 fragment at 130 °C for 25 min; the Raman spectra of this sample contain the same high frequency continuum of water and OH modes, where Raman intensities are reduced by approximately 20%. Raman spectra were also collected on the DSC run product that was heated to 800 °C; the results show no evidence of H_2O or OH modes. Therefore, the above Raman evidence indicates that the hydrous species Raman modes observed for the VHT altered sample (Fig. 5, top two plots) are mostly due to structural water or OH.

Similarities of the Raman features near 1640 cm^{-1}, and especially near 3545 cm^{-1}, for the VHT altered samples and analcime (Fig. 5) may indicate that some of the hydrous species incorporated into the amorphous portions of the VHT samples are part of the Na coordination environments within these samples. By calculating an eight oxygen normalized feldspar formula (e.g., albite: $NaAlSi_3O_8$) for the 3-day VHT samples, one finds that the composition of the Lo1AC2D3 and Lo2AC2D3 samples can be written as: $Na_{1.45}K_{0.05}Al_{0.31}B_{0.84}Si_{2.77}O_8{\cdot}0.68(H_2O)$ and $Na_{0.75}K_{0.11}Al_{0.29}B_{0.82}Si_3O_8{\cdot}1.40(H_2O)$, respectively. The water content of these VHT altered samples are similar to those found for analcime ($NaAlSi_3O_8{\cdot}1.5(H_2O)$ to $NaAlSi_{1.5}O_5{\cdot}0.5(H_2O)$) [10]. Water or OH bonding with Na^+ may be correlated with the expansion of the Na environment observed for the VHT samples as seen by Na X-ray absorption spectroscopy (see Section 5.2.4). A similar water–Na observation was made by Zotov and Keppler [16]: "... changes observed by neutron diffraction in the first coordination shell of Na^+ would be consistent with the formation of a hydration shell of H_2O molecules around this ion..."

Some consensus in the literature can be found with regard to the vibrational assignments behind the broad high frequency features, which segregate Si–OH (and possibly, Al–OH) stretch modes near 3580 cm^{-1} from lower frequency modes extending below 2350 cm^{-1} that are assigned to hydrogen bonding having various OH···O distances [12,15,16,20,21]. Frequency versus OH···O distance relationships have been determined for solutions and crystals containing this environment [21], where lower frequency features are assigned to longer OH···O distances. In the VHT altered sample spectra, bands near 3530 cm^{-1} can be assigned to Si–OH stretch modes, while the broad continuum of features between 3250 and 2340 cm^{-1} can be assigned to OH···O at distances ranging from 2.55 to longer than 2.75 Å [21].

5.2. X-ray absorption spectroscopy

5.2.1. Si XANES

Si XANES for all samples investigated are similar (Fig. 6a) and indicate SiO_4 tetrahedral environments. The spectrum for α-quartz (Fig. 6a, top) is similar to those presented earlier [33], where the edge peak, or white-line centroid energy was calibrated to 1846.8 eV. The Si K-edge centroids for the standards shift to slightly lower energies (1846.6 for analcime and leucite) as the crystal structures incorporate tetrahedral Al into the silicate tetrahedral framework; this trend is similar to that observed by Li et al. [33] for silica and aluminosilicate minerals. The spectra for the different standards show expected oscillation differences near the edge that are due to the different atomic arrangements surrounding Si within these crystal structures. The glass and VHT sample spectra are without most of the oscillations seen in the crystalline standards data (Fig. 6a, bottom three plots), which indicate more disordered atomic arrangements around Si within these amorphous samples than in the crystals (Fig. 6a, top three plots). White-lines for the glasses and VHT samples show a shift to slightly lower energies (1846.7–1846.5 eV) compared with α-quartz, consistent with the Al incorporation argument above [33]. Si XANES for the Lo1A and Lo2A glasses and VHT samples show similar trends, where the VHT sample edge peaks are at slightly lower energies (1846.5 eV) than those for the original glass (1846.7 eV). Since these samples have essentially the same Al_2O_3/SiO_2 ratios (Table 1), these edge energy trends may indicate decreased polymerization of the tetrahedral network [33] in the VHT altered samples with respect to the original glass, as observed by Raman spectroscopy (see Section 5.1.3).

5.2.2. Al XANES

The Al near-edge spectra were collected for analcime, leucite, the Lo glasses, and the corresponding VHT altered samples. Both crystalline standards analcime and leucite have tetrahedral Al, and have, as expected, one edge maximum near 1566 eV (Fig. 6b, top two plots). Spectra for the glasses and VHT samples are similar (Fig. 6b, bottom two sets of plots), have a single edge maximum near 1566 eV, and indicate tetrahedral Al coordinated by four oxygen atoms. The trends in the spectra show that the features do not shift much in energy, but the relative intensities of the peak (oscillation maximum) near 1570 eV do change. This amplitude damping for the Lo1A and Lo2A samples compared with the crystalline standards is most likely due to the larger structural disorder in these amorphous samples (glasses and VHT samples) versus that in the crystalline standards. There is also a slight sharpening of Al XANES interference features for the VHT altered samples compared with those for the original glasses, which may be due to slightly narrower distribution of Al–O distances within the VHT altered samples than those in the original glasses.

5.2.3. Na XANES

5.2.3.1. Analcime standard. The Na XANES spectrum for analcime (Figs. 6c and d) is similar to that presented earlier [22] and is more complex than that for any of the Lo samples (Fig. 6e). The two main edge features near 1076 and 1082 eV are similar to those observed for other crystalline aluminosilicates [24]. The more complicated features in the analcime data are due to the more ordered atomic arrangements around Na in this material than the Na environments in any of the predominantly amorphous Lo1A and Lo2A samples. Features near 1077, 1082, 1090, and 1110 eV are likely oscillation maxima due to interference effects from the structure surrounding Na, as shown by Na XANES calculations (Fig. 6c).

The structural differences around each Na-site lead to significant differences in the theoretical XANES, where the calculated spectrum for the Na(2)-site is a closer match to the experimental

data (Fig. 6d) than the calculation for Na(1). These results probably indicate that most Na within this particular analcime sample is in the Na(2)-sites [8]. Various calculated XANES mixtures for both Na-sites were generated, where the resulting spectra, that range from 100% Na(2) to 15% Na(1) + 85% Na(2), best match the XANES data.

As the Na(2) atomic cluster size was increased from the central absorbing atom, the calculated XANES features basically converged at a cluster radius (r_{max}) of 5.2 Å and larger (Fig. 6c). The 5.2 Å radius Na(2)-site cluster includes the $Na(H_2O)_2O_4$ local environment +2(Si at 3.17 Å) + 4(Si at 3.60 Å) + 4(Na at 4.19 Å) + 4(Si at 4.46 Å) + an array of 24 oxygen atoms at various distances. By restricting the cluster to r_{max} = 4.2 Å, only the oxygen nearest-neighbors, second nearest-neighbor Si atoms, and eight oxygens are included, where the feature near 1088 eV is absent. Only the nearest-neighbors are present in the r_{max} = 3.0 Å cluster, where the feature near 1077 eV is almost eliminated. These XANES findings for the analcime Na(2)-site provide insights into what surrounding atoms contribute to specific features in the Na XANES for the Lo1A and Lo2A samples.

5.2.3.2. Glasses and VHT samples. Na XANES spectra for the Lo1A and Lo2A samples have fewer features than that for analcime (Fig. 6e), and are similar to the Na XANES for Na-aluminosilicate glasses presented elsewhere [22]. The similarities of the energies of the main Na K-edge features for these samples indicate that the Na valence does not change. The overall shape of the Na XANES data changes considerably from silicate glasses [22], which have two features near 1077 and 1082 eV, to borate glasses [22], which have one broad edge maximum near 1079 eV. By using these observations, one can conclude that since the XANES data for the Lo1A and Lo2A samples contain two features near 1077 and 1081 eV, network-forming silicate tetrahedra dominate the Na nearest-neighbor environments, rather than borate units.

The trends observed for the analcime XANES calculations indicate that the two main Na XANES features for the Lo1A and Lo2A samples (Fig. 6e) are probably influenced by interference effects from the Na–O nearest-neighbor contributions (1082 eV peak), as well as second nearest-neighbor Na–Si contributions (1077 eV peak). XANES comparisons for the Lo1A and Lo2A samples show the largest change is the amplitude enhancement of the 1082 eV peak for the VHT altered samples with respect to the corresponding feature for the as-melted glasses (Fig. 6e); this change may indicate larger Na–O contributions for these samples.

5.2.4. Na EXAFS

5.2.4.1. Analcime standard. The $k^3\chi(k)$ data for analcime are more complex than those for the Lo glasses (Fig. 7a). The data for analcime contain relatively complicated oscillations (especially at low k) that indicate contributions from structural correlations beyond nearest-neighbor oxygen atoms, as shown in the corresponding RDF (Fig. 8a). The analcime RDF (Fig. 8a) has a prominent first-shell peak near 1.9 Å that is due to nearest-neighbor oxygen atoms (details given above), while a second-nearest-neighbor peak near 2.8 Å is due to Na–Si. The fit describes most of the major features in the $k^3\chi(k)$ and Na–O peak in the RDF data (Figs. 7a and 8a), but has deviations from the experimental Na–Si RDF peak near 2.8 Å. By using the assumption from the Na XANES calculations that most Na in the analcime sample is in the Na(2)-site, the EXAFS fitting results (Table 2) show that r_{Na-O} is within 0.03 Å and n is within 20% of the coordination number determined for Na(2) from the X-ray structure refinement [8]. The Na–Si EXAFS results do not correspond as well to the XRD findings [8], which may be due to interference effects in the second-nearest-neighbor peak from a longer distance Na–Si correlation (at 3.56 Å) that is not clearly observed in the RDF (Fig. 8a).

5.2.4.2. Glasses. The $k^3\chi(k)$ data for the Lo glasses are similar and are dominated by one frequency component that is damped compared with the analcime data (Fig. 7a). The RDFs for these glasses (Fig. 8a) have a nearest-neighbor peak near 1.9 Å and a smaller feature near 3.0 Å that may correspond to the Na–Si peak in the analcime RDF. Na–Si contributions in the EXAFS data are consistent with the finding of Na–Si dependent features in the XANES of these glasses. EXAFS fitting determined that these glasses have considerably shorter average Na–O distances and smaller coordination numbers than analcime (Table 2), but have similar r and n values to those determined for Na-silicate [25–27], Na-aluminosilicate [23,25], as well as (Na,Ca)-silicate glasses [26].

5.2.4.3. VHT samples. The $k^3\chi(k)$ data and corresponding RDFs for the VHT samples all show significantly larger amplitudes with respect to the corresponding glass data (Figs. 7b and 8b). For all VHT samples investigated, the $k^3\chi(k)$ oscillation period is slightly smaller than that for the corresponding as-melted glass, which transforms to longer distance nearest-neighbor RDF peaks than their glass counterparts. The fitting results indicate longer average Na–O distances by 0.05–0.10 Å, as well as an increase in n by as much as 70% versus the fitting parameters determined for the corresponding glass (Table 2). The Na–O coordination number increase in the VHT samples appears to correlate with the amplitude enhancement of the 1082 eV Na XANES feature for the VHT samples (Fig. 6e) assigned to Na–O nearest-neighbor contributions. RDF comparisons of the VHT samples with respect to their glass counterparts (Fig. 8b), indicate changes in the Na–Si peaks (near 3.0 Å) are minimal, at best, with respect to the significant differences in the Na–O peaks (near 1.9 Å); this observation also correlates with the relatively unchanged amplitudes of the 1077 eV XANES peak (assigned to Na–Si) with respect to the noticeable differences with the 1082 eV XANES peak (assigned to Na–O) (Fig. 6e, bottom two sets of plots). EXAFS fitting results for the VHT altered samples (Fig. 9a and b, Table 2) describe most of the features in the $k^3\chi(k)$ data and corresponding RDFs. With respect to the original glasses, the EXAFS data and analyses results indicate the VHT altered samples contain expanded Na environments with longer Na–O distances and more oxygen nearest-neighbors.

6. Conclusions

Raman and X-ray absorption spectroscopies are used to characterize structural changes that took place in (Na,K) borosilicate glasses during exposure to hydrothermal conditions in vapor hydration tests for three and 20 days at 200 °C. Raman spectroscopy, XRD, and SEM indicate that the VHT samples are mostly amorphous with minor amounts of analcime-like and leucite-like crystals near the sample surfaces. SEM and DSC analyses of these samples indicate significant Na_2O depletion, some B_2O_3 enrichment (Table 1), and significant incorporation of water or OH in the VHT altered samples with respect to their as-melted glasses. Raman indicates that the glass structural changes are the same for samples exposed to the 3-day and 20-day VHT; these changes include partial depolymerization of the borosilicate network, as well as incorporation of hydrous species into the glass structure. Al and Si XANES data indicate network-forming Al and Si tetrahedral environments in all glasses and VHT samples investigated. However, slight energy shifts in the Si K-edge data also indicate that the altered VHT samples may have less polymerized tetrahedra than the original glasses. Due to charge balancing considerations in the glass structures, Al tetrahedra in the aluminosilicate tetrahedral networks may be near Na environments. The slightly less structurally disordered Al tetrahedra in the VHT altered samples, as shown by Al XANES, may be a tetrahedral network

adjustment to changes in the Na environments. Na EXAFS for the Lo glasses indicate average Na–O distances from 2.27 to 3.31 Å, with three to four nearest-neighbor oxygen atoms; after VHT alteration, the Na environments expand, where the Na–O distances lengthen by as much as 0.10 Å and coordination numbers can increase to five. Raman spectra of the samples investigated here provide additional information about the Na-environment differences in the Lo samples. Raman data indicate no evidence of hydrous species in the original glasses, but the VHT altered samples have H_2O- or OH-associated features similar to those observed for analcime, where Na-sites contain H_2O. The low SEM–WDS composition totals, DSC findings, and the Raman observations indicate that the expanded Na environments in the VHT samples may contain oxygen atoms associated with water or OH. The hydrous species in the VHT samples are probably within a wide variety of environments that include: (Si,Al)–OH, OH$\cdots$O bonds at various distances, as well as H_2O or OH coordinating with Na. Differences in Na/K ratios have little to no structural effect on the as-melted glasses or the structural changes observed between the original glasses and the corresponding VHT altered samples.

Acknowledgments

We thank Frank Lofaj (Vitreous State Laboratory) for preparation of the glasses [1] that were tested and characterized in this work. We also thank Jeffrey Post and Paul Pohwat (Mineral Sciences Department, Smithsonian Institution) for providing the quartz, analcime, and leucite crystals. The assistance of D.K. Shuh and P. Nachimuthu (LBNL), as well as M. Laurenzi (VSL) during the XAS data collection at ALS Beam Line 6.3.2 is also appreciated.

References

[1] A.C. Buechele, F. Lofaj, I.S. Muller, C.T.F. Mooers, I.L. Pegg, Ceram. Trans. 155 (2004) 289.
[2] ASTM C1663-09, Standard Test Method for Measuring Waste Glass or Glass Ceramic Durability by Vapor Hydration Test, Copyright 2009, ASTM International, 100 Barr Harbour Dr., P.O. Box C-700 West Conshohocken, Pennsylvania 19428-2959, United States.
[3] A.C. Buechele, F. Lofaj, C. Mooers, I.L. Pegg, Ceram. Trans. 132 (2002) 301.
[4] A. Ledieu, F. Devreux, P. Barboux, L. Sicard, O. Spalla, J. Non-Cryst. Solids 343 (2004) 3.
[5] S. Ribet, S. Gin, J. Nucl. Mater. 324 (2004) 152.
[6] N. Tsomaia, S.L. Brantley, J.P. Hamilton, C.G. Pantano, K.T. Mueller, Am. Mineral. 88 (2003) 54.
[7] J.P. Hamilton, C.G. Pantano, J. Non-Cryst. Solids 222 (1997) 167.
[8] F. Mazzi, E. Galli, Am. Mineral. 63 (1978) 448.
[9] B. Winkler, M.T. Dove, M. Leslie, Am. Mineral. 76 (1991) 313.
[10] P. Saha, Am. Mineral. 44 (1959) 300.
[11] W.A. Deer, R.A. Howie, J. Zussman, Rock Forming Minereral, vol. 4, 1962, p. 341 (and 4B (2004) 542).
[12] P.F. McMillan, R.L. Remmele, Am. Mineral. 71 (1986) 772.
[13] D.W. Matson, S.K. Sharma, J.A. Philpotts, Am. Mineral. 71 (1986) 694.
[14] D.A. McKeown, F.L. Galeener, G.E. Brown Jr., J. Non-Cryst. Solids 68 (1984) 361.
[15] N. Zotov, H. Keppler, Phys. Chem. Miner. 25 (1998) 259.
[16] N. Zotov, H. Keppler, Am. Mineral. 83 (1998) 823.
[17] F.L. Galeener, J. Non-Cryst. Solids 49 (1982) 53.
[18] P.F. McMillan, B.T. Poe, T.R. Stanton, R.L. Remmele, Phys. Chem. Miner. 19 (1993) 454.
[19] E.I. Kamitsos, M.A. Karakassides, G.D. Chryssikos, J. Chem. Phys. 90 (1986) 4528.
[20] R. Thomas, Am. Mineral. 85 (2000) 868.
[21] K. Nakamoto, M. Margoshes, R.E. Rundle, J. Am. Chem. Soc. 77 (1955) 6480.
[22] D.R. Neuville, L. Cormier, A.-M. Flank, R.J. Prado, P. LaGarde, Eur. J. Mineral. 16 (2004) 809.
[23] B.P. McGrail, J.P. Icenhower, D.K. Shuh, P. Liu, J.G. Darab, D.R. Baer, S. Thevuthasen, V. Shutthanandan, M.H. Engelhard, C.H. Booth, P. Nachimuthu, J. Non-Cryst. Solids 296 (2001) 10.
[24] A. Mottana, T. Murata, Z.Y. Wu, A. Marcelli, E. Paris, Phys. Chem. Miner. 24 (1997) 500.
[25] G.N. Greaves, K.L. Ngai, Phys. Rev. B 52 (1995) 6358.
[26] G.N. Greaves, A. Fontaine, P. Lagarde, D. Raoux, S.J. Gurman, Nature 293 (1981) 911.
[27] C. Mazzara, J. Jupille, A.-M. Flank, P. Lagarde, J. Phys. Chem. B 104 (2000) 3438.
[28] D.A. McKeown, G.A. Waychunas, G.E. Brown, J. Non-Cryst. Solids 74 (1985) 325.
[29] D.A. McKeown, G.A. Waychunas, G.E. Brown, J. Non-Cryst. Solids 74 (1985) 349.
[30] D.A. McKeown, Phys. Chem. Miner. 16 (1989) 678.
[31] J.A. van Bokhoven, T. Nabi, H. Sambe, D.E. Ramaker, D.C. Koningsberger, J. Phys.: Condens. Matter. 13 (2001) 10247.
[32] Z. Wu, C. Romano, A. Marcelli, A. Motanna, G. Cibin, G. Della Ventura, G. Giuli, P. Courtial, D.B. Dingwell, Phys. Rev. B 60 (1999) 9216.
[33] D. Li, G.M. Bancroft, M.E. Fleet, X.H. Feng, Phys. Chem. Miner. 22 (1995) 115.
[34] D. Li, G.M. Bancroft, M. Kasrai, M.E. Fleet, R.A. Secco, X.H. Feng, K.H. Tan, B.X. Yang, Am. Mineral. 79 (1994) 622.
[35] A.F. Goncharov, V.V. Struzhkin, J. Raman Spectrosc. 34 (2003) 538.
[36] M. Born, K. Huang, Dynamical Theory of Crystal Lattices, Clarendon, Oxford, 1954. pp. 199–204.
[37] F.L. Galeener, P.N. Sen, Phys. Rev. B 17 (1978) 1928.
[38] D.E. Sayers, B.A. Bunker, in: D.C. Kroningsberger, R. Prins (Eds.), X-ray Absorption Principles, Applications, Techniques of EXAFS, SEXAFS, and XANES, Wiley, New York, 1988. p. 211.
[39] D. Haskel, The Executable Code and Documentation. <http://www.aps.anl.gov/xfd/people/haskel/fluo.html>, 1999.
[40] J.J. Rehr, R.C. Albers, Rev. Mod. Phys. 72 (2000) 621.
[41] M. Newville, B. Ravel, D. Haskel, E.A. Stern, Y. Yacoby, Physica B 208–209 (1995) 154.
[42] P.A. Lee, G. Beni, Phys. Rev. B 15 (1977) 2862.
[43] C.H. Booth, F. Bridges, Phys. Scr. T 115 (2005) 202.
[44] S.I. Zabinsky, J.J. Rehr, A. Ankudinov, R.C. Albers, M.J. Eller, Phys. Rev. Lett. B 52 (1995) 2995.
[45] C.V. Putnis, T. Geister, P. Schmid-Beurmann, T. Stephan, C. Giampaolo, Am. Mineral. 92 (2007) 19.
[46] B. Wopenka, J.J. Freeman, T. Nikischer, Appl. Spectrosc. 52 (1998) 54.
[47] C.M.B. Line, A. Putnis, C. Putnis, C. Giampaolo, Am. Mineral. 80 (1995) 268.